Available online at www.sciencedirect.com
ScienceDirect
Journal of Sound and Vibration 310 (2008) 409–420
JOURNAL OF SOUND AND VIBRATION
www.elsevier.com/locate/jsvi

Vibration isolation using buckled or pre-bent columns—Part 1: Two-dimensional motions of horizontal rigid bar

R.H. Plaut[a,*], H.M. Favor[a], A.E. Jeffers[a], L.N. Virgin[b]

[a]*The Charles E. Via, Jr., Department of Civil and Environmental Engineering, Virginia Polytechnic Institute and State University, Blacksburg, VA 24061-0105, USA*

[b]*Department of Civil and Environmental Engineering, Duke University, Durham, NC 27708-0287, USA*

Received 20 May 2006; received in revised form 17 September 2007; accepted 25 September 2007
Available online 31 October 2007

Abstract

The use of buckled columns, or pairs of pre-bent columns bonded with a viscoelastic filler, as vibration isolators is analyzed. They support a horizontal rigid bar at its ends, and harmonic vertical motion is applied at the base of the isolators. The displacement transmissibility is analyzed for both symmetric and asymmetric bars. In the latter case, the bar exhibits rotational as well as translational motion. Each column is modeled as an elastica, allowing for large deflections. Small steady-state vibrations about the equilibrium configuration of the system are analyzed. After formulation of the governing equations, a shooting method is utilized to obtain numerical solutions in Mathematica. The transmissibility is plotted as a function of the excitation frequency, and vibration shapes associated with peaks in the transmissibility plots are shown. For the buckled single-column isolators, the effect of the amount of asymmetry of the bar is examined. For the bonded two-column pre-bent isolators, the effects of the filler stiffness, amount of initial curvature, and supported weight are determined. The isolators can be effective for a large range of excitation frequencies.

1. Introduction

Winterflood and collegues [1–5] have studied the application of buckled columns, called Euler springs, as vibration isolators. These devices may be efficient by having relatively low mass and stored energy while supporting weights statically, and then a large isolation bandwidth due to their vibration characteristics. The application of interest was low-frequency isolation of the Australian International Gravitational Observatory.

Virgin and Davis [6] conducted experiments with a weight supported by two buckled pinned–pinned columns. The system was effective when the frequency of the vertical harmonic base excitation was sufficiently high. Plaut et al. [7] analyzed an isolator consisting of two rigid bars connected with a rotational spring, and included responses with large isolator motions caused by parametric and external (forcing) terms in the governing equations. Buckled and pre-bent columns with fixed ends were examined in Plaut et al. [8]. A weight was supported by a single column, and the deflection transmissibility (i.e., the amplitude of the motion of the

*Corresponding author. Tel.: +1 540 231 6072; fax: +1 540 231 7532.
E-mail address: rplaut@vt.edu (R.H. Plaut).

0022-460X/$ - see front matter © 2007 Elsevier Ltd. All rights reserved.
doi:10.1016/j.jsv.2007.09.037

weight divided by the amplitude of the motion of the base of the column) was computed over a range of excitation frequencies. The effects of external and internal damping, column stiffness, supported weight, and initial curvature were investigated. Two-frequency base excitations were also applied.

Finally, Bonello et al. [9] considered the use of curved beams with pinned ends. The beams had a piezoelectric layer between a steel layer and an aluminum layer. Vertical motion of a mass supported by two of the isolators was analyzed. The curvatures of the beam could be adjusted during motion of the system to vary the vertical stiffness and reduce the force transmissibility. Tests were conducted to demonstrate the effectiveness of the adaptive tuned vibration absorber.

The present analysis extends previous work by considering a horizontal rigid bar supported at its ends by such isolators, and allowing for rotational as well as vertical motions. The displacement transmissibility is investigated. Single-column isolators that are slightly buckled by the weight of the bar are treated first. The bar may be symmetric or asymmetric. Then two-column isolators that are pre-bent and bonded together by a viscoelastic filler are investigated in the case of a symmetric bar. It is desired to have large ranges of applied frequency for which the transmissibility is very low.

2. Formulation for single-column isolators

2.1. Variables and parameters

For a single column supporting each end of the rigid bar, the system is depicted in Fig. 1. Each column is assumed to be an elastica, which is thin, flexible, inextensible, and unshearable [10]. Column j is uniform with constant bending stiffness $\alpha_j EI_c$, constant mass per unit length $\alpha_j \mu$, and length L. (For cases in which the columns are not identical, i.e., $\alpha_j \neq 1$, it is assumed that their thicknesses are the same and widths are different, so that the bending stiffness is proportional to the mass per unit length.) The weights of the columns are neglected. From the base, the arc length is S_j, the axial and transverse coordinates are $X_j(S,T)$ and $Y_j(S,T)$, respectively, and the rotation angle in radians is $\theta_j(S,T)$, where T denotes time. The columns are unstrained when they are straight. In equilibrium, the fraction of the weight of the rigid bar acting on each column is

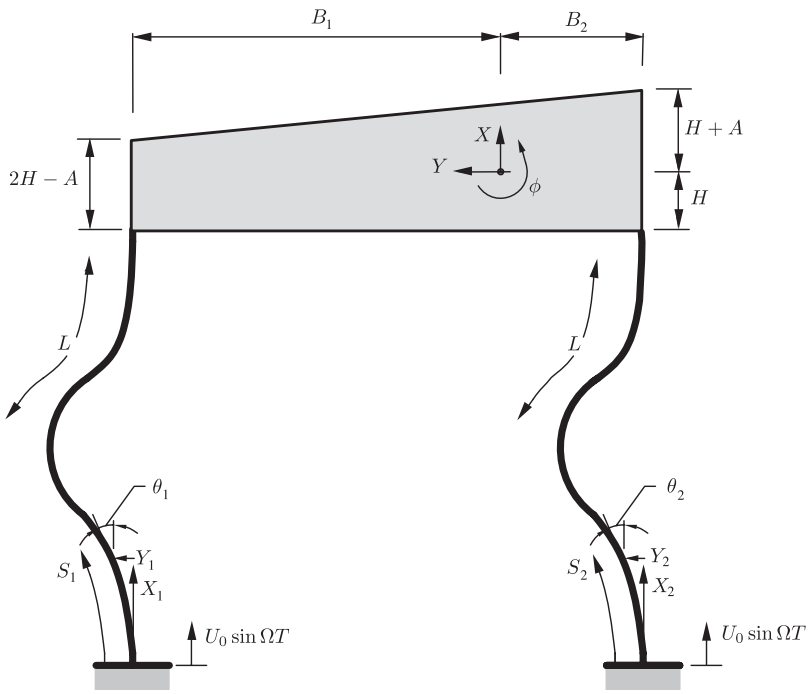

Fig. 1. Geometry of rigid bar with single-column isolators.

slightly higher than the critical load for that column, and the columns are assumed to be buckled outward in the numerical work. External damping with coefficient C is assumed to act on the columns. The applied vertical deflection at the base of each column is $U_0 \sin \Omega T$, positive if upward, with $U_0 > 0$.

The bar is assumed to have a trapezoidal shape, and in equilibrium its bottom edge is horizontal. The bar's thickness is $2H-A$ at the left edge and $2H+A$ at the right edge, and its weight is $2P_0$. Its centroid is located at a distance H above the bottom edge and at distances B_1 and B_2 from the sides, as shown in Fig. 1, so that, in terms of the total bar length and the parameters in the side dimensions, $B_1 = (6H+A)(B_1+B_2)/(12H)$ and $B_2 = (6H-A)L/(12H)$. From equilibrium, the vertical deflection of the bar is denoted $X(T)$, the horizontal deflection is $Y(T)$, and the rotation is $\phi(T)$, with positive senses shown in Fig. 1. It is assumed that the horizontal deflection is constrained to be zero in equilibrium, and in the vibration results it turns out to be very small.

The components of the internal force in column j along the fixed X_j and Y_j directions are denoted $P_j(S,T)$ and $Q_j(S,T)$, respectively, and the bending moment is $M_j(S,T)$. Fig. 2 shows a free body diagram of an element of the column, including inertia and damping forces. The subscript j and coefficient α_j are not included, and the superscript $+$ denotes quantities at arc length $S+\mathrm{d}S$.

2.2. Equations for columns

The two geometrical relationships, the constitutive law, and the three equations of motion for column j are as follows:

$$\frac{\partial X_j}{\partial S_j} = \cos\,\theta_j, \quad \frac{\partial Y_j}{\partial S_j} = \sin\,\theta_j, \quad \frac{\partial \theta_j}{\partial S_j} = \frac{M_j}{\alpha_j \mathrm{EI}_c}, \quad \frac{\partial M_j}{\partial S_j} = Q_j \cos\,\theta_j - P_j \sin\,\theta_j,$$
$$\frac{\partial P_j}{\partial S_j} = -\alpha_j \mu \frac{\partial^2 X_j}{\partial T^2} - C\frac{\partial X_j}{\partial T}, \quad \frac{\partial Q_j}{\partial S_j} = -\alpha_j \mu \frac{\partial^2 Y_j}{\partial T^2} - C\frac{\partial Y_j}{\partial T} \quad (j = 1,2). \tag{1}$$

Small motions about equilibrium will be considered. The subscript "e" will denote quantities in the equilibrium state, and the subscript "d" will denote dynamic quantities. The column variables are written in the following complex form:

$$X_j(S_j,T) = X_{je}(S_j) + X_{jd}(S_j)\,\mathrm{e}^{\mathrm{i}\Omega T}, \quad Y_j(S_j,T) = Y_{je}(S_j) + Y_{jd}(S_j)\,\mathrm{e}^{\mathrm{i}\Omega T},$$
$$\theta_j(S_j,T) = \theta_{je}(S_j) + \theta_{jd}(S_j)\,\mathrm{e}^{\mathrm{i}\Omega T}, \quad M_j(S_j,T) = M_{je}(S_j) + M_{jd}(S_j)\,\mathrm{e}^{\mathrm{i}\Omega T},$$
$$P_j(S_j,T) = P_{je} + P_{jd}(S_j)\,\mathrm{e}^{\mathrm{i}\Omega T}, \quad Q_j(S_j,T) = Q_{je} + Q_{jd}(S_j)\,\mathrm{e}^{\mathrm{i}\Omega T} \quad (j = 1,2). \tag{2}$$

The imaginary parts of the dynamic variables will correspond to the response to the excitation.

In equilibrium, the last two of Eqs. (1) imply that the internal force components, P_{je} and Q_{je}, are constant along the column. The other equations are

$$\frac{\mathrm{d}X_{je}}{\mathrm{d}S_j} = \cos\,\theta_{je}, \quad \frac{\mathrm{d}Y_{je}}{\mathrm{d}S_j} = \sin\,\theta_{je}, \frac{\mathrm{d}\theta_{je}}{\mathrm{d}S_j} = \frac{M_{je}}{\alpha_j \mathrm{EI}_c},$$
$$\frac{\mathrm{d}M_{je}}{\mathrm{d}S_j} = Q_{je}\cos\,\theta_{je} - P_{je}\sin\,\theta_{je} \quad (j = 1,2). \tag{3}$$

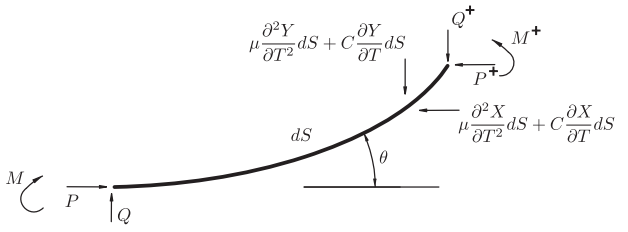

Fig. 2. Free body diagram of column element, including inertia and external damping forces.

For small steady-state vibrations about equilibrium, Eqs. (1) and (2) lead to the following governing linear equations in the dynamic variables:

$$\frac{dX_{jd}}{dS_j} = -\theta_{jd} \sin\theta_{je}, \quad \frac{dY_{jd}}{dS_j} = \theta_{jd} \cos\theta_{je}, \quad \frac{d\theta_{jd}}{dS_j} = \frac{M_{jd}}{\alpha_j EI_c},$$
$$\frac{dM_{jd}}{dS_j} = (Q_{jd} - P_{je}\theta_{jd})\cos\theta_{je} - (P_{jd} + Q_{je}\theta_{jd})\sin\theta_{je},$$
$$\frac{dP_{jd}}{dS_j} = (\alpha_j \mu\Omega^2 - i\Omega C)X_{jd},$$
$$\frac{dQ_{jd}}{dS_j} = (\alpha_j \mu\Omega^2 - i\Omega C)Y_{jd} \quad (j = 1, 2). \tag{4}$$

2.3. Equations for rigid bar

The moment of inertia of the rigid bar about its centroid is given by

$$I = \frac{P_0}{72gH^2}[(12H^2 - A^2)(B_1 + B_2)^2 + 48H^4 + 24H^2A^2 - A^4], \tag{5}$$

where g denotes gravitational acceleration. A free body diagram of the bar is shown in Fig. 3. The three equations of motion for the bar are

$$\frac{2P_0}{g}\frac{d^2X(T)}{dT^2} = P_1(L,T) + P_2(L,T) - 2P_0, \tag{6}$$

$$\frac{2P_0}{g}\frac{d^2Y(T)}{dT^2} = Q_1(L,T) + Q_2(L,T), \tag{7}$$

$$I\frac{d^2\phi(T)}{dT^2} = [P_2(L,T)B_2 - P_1(L,T)B_1 - Q_2(L,T)H - Q_1(L,T)H]\cos\phi(T)$$
$$+ [P_2(L,T)H + P_1(L,T)H + Q_2(L,T)B_2 - Q_1(L,T)B_1]\sin\phi(T)$$
$$- M_1(L,T) - M_2(L,T). \tag{8}$$

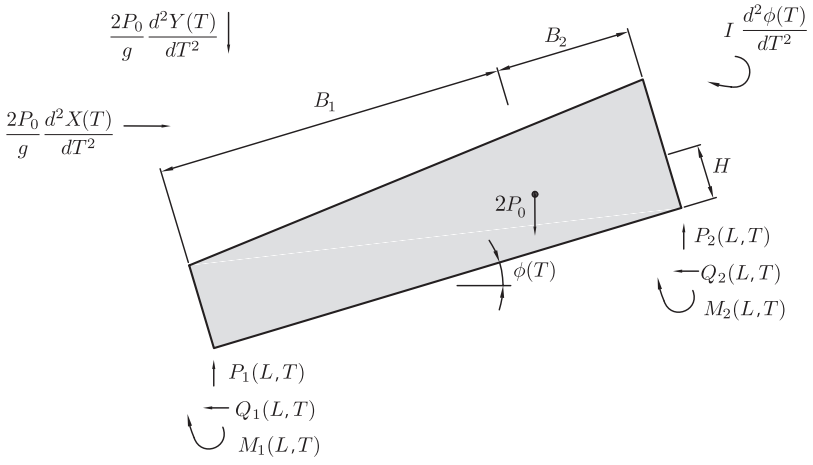

Fig. 3. Free body diagram of rigid bar, including inertia forces.

From geometrical considerations,

$$\begin{aligned} X_{1e}(L) + H + X(T) &= X_1(L,T) + H\cos\phi(T) + B_1\sin\phi(T) \\ &= X_2(L,T) + H\cos\phi(T) - B_2\sin\phi(T) \end{aligned} \tag{9}$$

and

$$\begin{aligned} B_2 + Y(T) &= Y_2(L,T) + H\sin\phi(T) + B_2\cos\phi(T) \\ &= B_1 + B_2 + Y_1(L,T) + H\sin\phi(T) - B_1\cos\phi(T). \end{aligned} \tag{10}$$

Eqs. (9) and (10) lead to the expressions

$$\sin\phi(T) = \frac{X_2(L,T) - X_1(L,T)}{B_1 + B_2}, \tag{11}$$

$$\cos\phi(T) = \frac{B_1 + B_2 + Y_1(L,T) - Y_2(L,T)}{B_1 + B_2} \tag{12}$$

and

$$X(T) = \frac{X_1(L,T)B_2 + X_2(L,T)B_1 + Y_1(L,T)H - Y_2(L,T)H - (B_1 + B_2)L}{B_1 + B_2}, \tag{13}$$

$$Y(T) = \frac{Y_1(L,T)B_2 + Y_2(L,T)B_1 + X_2(L,T)H - X_1(L,T)H}{B_1 + B_2}. \tag{14}$$

Steady-state motions of the rigid bar about equilibrium are written as

$$X(T) = X_d\,\mathrm{e}^{\mathrm{i}\Omega T}, \quad Y(T) = Y_d\,\mathrm{e}^{\mathrm{i}\Omega T}, \quad \phi(T) = \phi_d\,\mathrm{e}^{\mathrm{i}\Omega T}. \tag{15}$$

Linearizing Eq. (11) and using $X_{2e} = X_{1e}$, the rotational amplitude ϕ_d can be written in terms of the column variables as

$$\phi_d = \frac{X_{2d}(L) - X_{1d}(L)}{B_1 + B_2}. \tag{16}$$

2.4. Boundary conditions and transmissibility

Eqs. (13)–(16) are used with Eqs. (6)–(8) to eliminate X, Y, and ϕ in the boundary conditions at the tops of the columns. For equilibrium, those boundary conditions at $S_j = L$ are

$$\begin{aligned} &X_{2e} = X_{1e}, \quad Y_{je} = 0, \quad \theta_{je} = 0, \quad P_{1e} + P_{2e} = 2P_0, \\ &Q_{je} = 0, \quad P_{2e}B_2 - P_{1e}B_1 = M_{1e} + M_{2e} \quad (j = 1,2). \end{aligned} \tag{17}$$

For the dynamic variables, the boundary conditions at $S_j = L$ are

$$\begin{aligned} &Y_{2d} = Y_{1d}, \quad \theta_{1d} = \frac{X_{2d} - X_{1d}}{B_1 + B_2}, \quad \theta_{2d} = \theta_{1d}, \\ &-2\Omega^2 P_0(X_{1d}B_2 + X_{2d}B_1) = (B_1 + B_2)(P_{1d} + P_{2d})g, \\ &-2\Omega^2 P_0(Y_{1d}B_2 + Y_{2d}B_1 + X_{2d}H - X_{1d}H) = (B_1 + B_2)(Q_{1d} + Q_{2d})g, \\ &hskip - 28pt - \Omega^2 I(X_{2d} - X_{1d}) = (2P_0H + Q_{2e}B_2 - Q_{1e}B_1)(X_{2d} - X_{1d}) \\ &hskip - 28pt \quad + (B_1 + B_2)(P_{2d}B_2 - P_{1d}B_1 - Q_{2d}H - Q_{1d}H - M_{1d} - M_{2d}). \end{aligned} \tag{18}$$

At $S_j = 0$, $X_{je} = Y_{je} = \theta_{je} = Y_{jd} = \theta_{jd} = 0$ and $X_{jd} = U_0$.

The transmissibility (TR) of interest here is the ratio of the amplitude of the vertical motion of the center of the bar to the amplitude U_0 of the applied vertical base motion. Therefore

$$TR = \frac{1}{2U_0}\sum_{j=1}^{2}\sqrt{\{\mathrm{Re}\,[X_{jd}(L)]\}^2 + \{\mathrm{Im}\,[X_{jd}(L)]\}^2}. \tag{19}$$

This transmissibility is independent of U_0.

The calculations are carried out in terms of the nondimensional quantities

$$b_j = \frac{B_j}{L}, \quad h = \frac{H}{L}, \quad a = \frac{A}{L}, \quad x_j = \frac{X_j}{L}, \quad y_j = \frac{Y_j}{L}, \quad s_j = \frac{S_j}{L}, \quad p_0 = \frac{P_0 L^2}{EI_c},$$
$$p_j = \frac{P_j L^2}{EI_c}, \quad q_j = \frac{Q_j L^2}{EI_c}, \quad m_j = \frac{M_j L}{EI_c}, \quad u_0 = \frac{U_0}{L}, \quad r = \frac{EI_c}{\mu g L^3}, \quad c = \frac{CL^2}{\sqrt{\mu EI_c}},$$
$$t = \frac{T\sqrt{EI_c}}{L^2\sqrt{\mu}}, \quad \omega = \frac{\Omega L^2\sqrt{\mu}}{\sqrt{EI_c}} \quad (j = 1, 2). \tag{20}$$

For equilibrium and then for vibrations, numerical solutions are obtained using a shooting method with the software Mathematica [11]. In the numerical examples in the following section:

$$b_1 + b_2 = 1, \quad h = 0.1, \quad p_0 = 40, \quad r = 1, \quad c = 1, \quad u_0 = 0.01. \tag{21}$$

Therefore the length of the bar is the same as the length of each column, the aspect ratio in the case of a uniform bar is 0.2, and in equilibrium the axial load in each column is 1.3 percent higher than its critical load. The quantity r is called the stiffness parameter. As mentioned before, the value specified for u_0 does not affect the results.

3. Results for single-column isolators

The case of a uniform bar is considered first, so that $\alpha_j = 1$, $b_1 = 0.5$, and $\phi = 0$. The results are the same as for the problem treated in Ref. [8] involving a single column supporting a mass. A single column, e.g., $j = 1$, can be analyzed. For equilibrium, $p_{1e} = p_0$, $q_{1e} = 0$, and, at $s = 0$, $x_{1e} = y_{1e} = \theta_{1e} = 0$. Using Eqs. (3) in nondimensional form, the "initial condition" $m_{1e}(0)$ is varied until $y_{1e}(1) = 0$ and $\theta_{1e}(1) = 0$ with sufficient accuracy. Using Eqs. (4) in nondimensional form, in the dynamic part of the analysis, $x_{1d}(0) = u_0$, $y_{1d}(0) = \theta_{1d}(0) = 0$, and $m_{1d}(0)$, $p_{1d}(0)$ and $q_{1d}(0)$ are varied until $y_{1d}(1) = \theta_{1d}(1) = 0$, and $p_{1d}(1) = -\omega^2 r p_0 x_{1d}(1)$.

The transmissibility curve is shown in Fig. 4, in which TR is plotted as a function of the nondimensional excitation frequency ω for $0.1 < \omega < 200$ using log scales. The curve for the range $0.1 < \omega < 15$ was included in Ref. [8]. The first peak occurs at $\omega = 0.698$, and the corresponding steady-state vibration shape is depicted in Fig. 5(a). The columns exhibit no nodes in this shape, and the dynamic shape is symmetric about midspan.

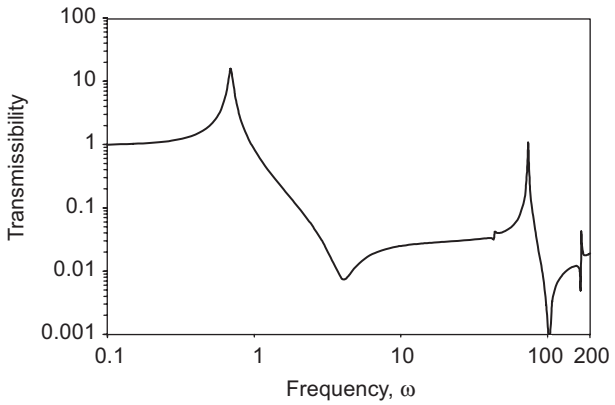

Fig. 4. Transmissibility curves for symmetric bar; $0.1 < \omega < 200$.

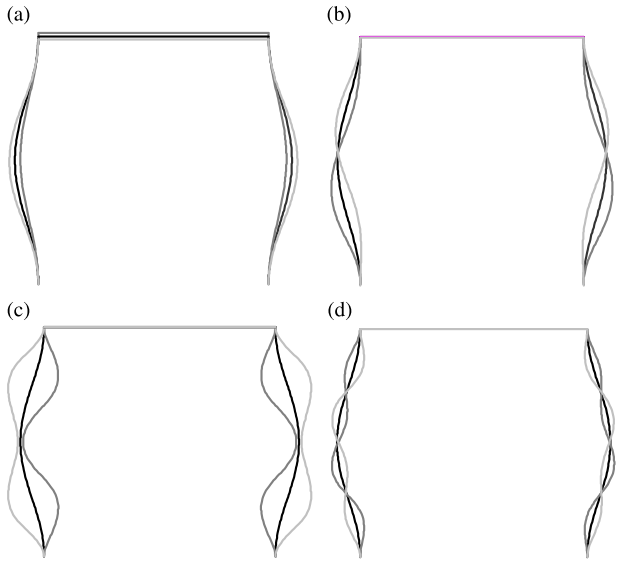

Fig. 5. Steady-state vibration shapes at peak frequencies: (a) $\omega = 0.698$, (b) $\omega = 44.73$, (c) $\omega = 75.26$ and (d) $\omega = 173.6$.

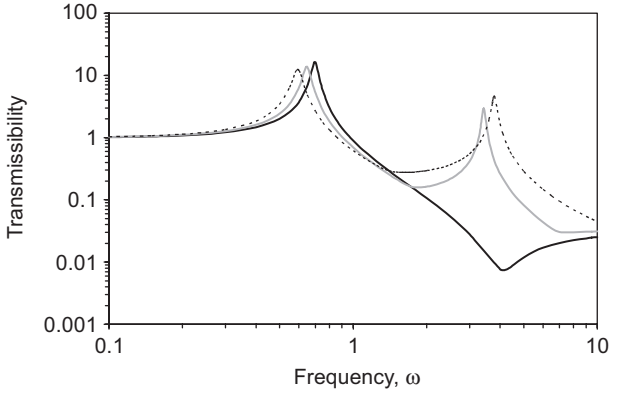

Fig. 6. Transmissibility curves for asymmetric bar; $0.1 < \omega < 10$: light solid curve, $b_1 = 0.50$; dark solid curve, $b_1 = 0.55$; and dotted curve, $b_1 = 0.70$.

There is a small peak in TR at $\omega = 44.73$, and the column vibration shapes shown in Fig. 5(b) are anti-symmetric about equilibrium, with only a node at midspan. For the peak at $\omega = 75.26$, the columns vibrate in a symmetric dynamic shape with no nodes (Fig. 5(c)), so that all points pass through the equilibrium configuration simultaneously. The shapes corresponding to the peak at $\omega = 173.6$ have three nodes and are anti-symmetric about equilibrium, as seen in Fig. 5(d).

Next, the bar is assumed to be asymmetric with $b_1 > b_2$. For equilibrium, x_{je}, y_{je}, and θ_{je} are zero at $s_j = 0$, $p_{je} = \alpha_j p_0$ (with $\alpha_2 = 2 - \alpha_1$), and $q_{je} = 0$ ($j = 1,2$). Using Eq. (3), the quantities $m_{je}(0)$ and α_1 are varied until Eqs. (17) are satisfied in nondimensional form at $s_j = 1$. The cases $b_1 = 0.55$, 0.60, 0.65, and 0.70 are considered. The corresponding values of α_1 are 0.9093, 0.8183, 0.7278, and 0.6370, respectively. For example, if $b_1 = 0.55$, the bending stiffnesses in the left and right columns in Fig. 1 are $0.9093EI_c$ and $1.0907EI_c$, respectively, and the corresponding axial loads in equilibrium are $40(0.9093) = 36.37$ and $40(1.0907) = 43.63$.

Using Eqs. (4), for the dynamic analysis of the asymmetric bar, $x_{jd}(0) = u_0$, $y_{jd}(0) = \theta_{jd}(0) = 0$, and $m_{jd}(0)$, $p_{jd}(0)$ and $q_{jd}(0)$ are varied until Eqs. (18) are satisfied in nondimensional form. The effect of asymmetry is illustrated in Fig. 6 for a small range of excitation frequency ($0.1 < \omega < 10$). Transmissibility plots are presented for $b_1 = 0.50$ (as in Fig. 4), 0.55, and 0.70. The excitation frequency at the first peak does not vary

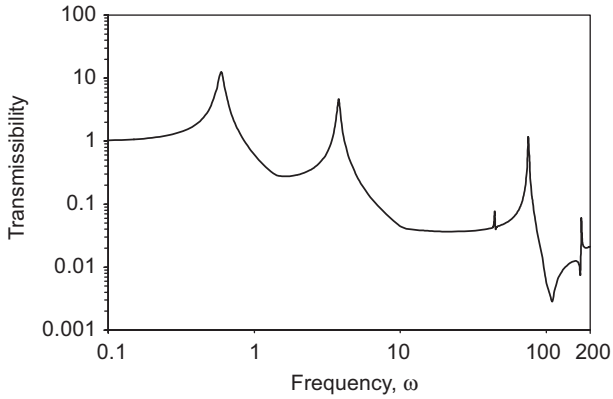

Fig. 7. Transmissibility curve for asymmetric bar; $b_1 = 0.70$, $0.1 < \omega < 200$.

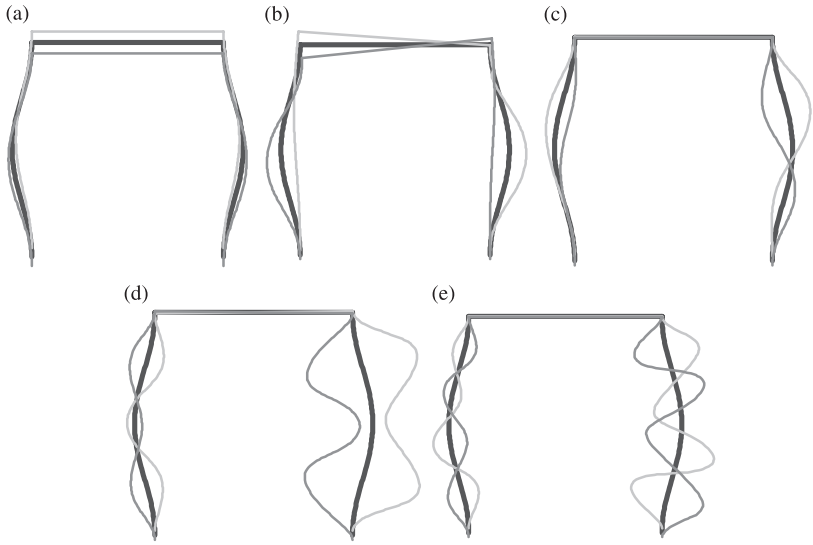

Fig. 8. Steady-state vibration shapes at peak frequencies for $b_1 = 0.70$: (a) $\omega = 0.59$, (b) $\omega = 3.79$, (c) $\omega = 44.3$, (d) $\omega = 75.3$, and (e) $\omega = 173.6$.

monotonically with b_1. For $b_1 = 0.50$, 0.55, 0.60, 0.65, and 0.70, respectively, the first peak occurs at $\omega = 0.698$, 0.710, 0.646, 0.646, and 0.593. An additional transmissibility peak is exhibited if the bar is asymmetric. For $b_1 = 0.55$, 0.60, 0.65, and 0.70, respectively, it occurs at $\omega = 3.277$, 3.430, 3.516, and 3.789.

A larger range of frequency, $0.1 < \omega < 200$, is used in Fig. 7 for the case $b_1 = 0.70$, and the shapes associated with the transmissibility peaks are plotted in Fig. 8. At $\omega = 0.593$, the bar exhibits little rotation, so that the motion is mostly vertical. At $\omega = 3.789$, the bar rotates significantly, with a node near its right end. For the small peak at $\omega = 44.31$ and the peaks at $\omega = 75.28$ and 173.6, there is little rotation of the bar, and the amplitude of motion of the right column is much larger than that of the left column. In Fig. 8(d), with $\omega = 75.28$, the vibration shape of the right column has three local extrema but no nodes, as seen in some other problems [12,13].

4. Formulation for two-column isolators

Now the system shown in Fig. 9 is considered. Each isolator consists of two pre-bent columns bonded together with a filler that provides stiffness and damping. The rigid bar is uniform and has weight $4P_0$. The bar

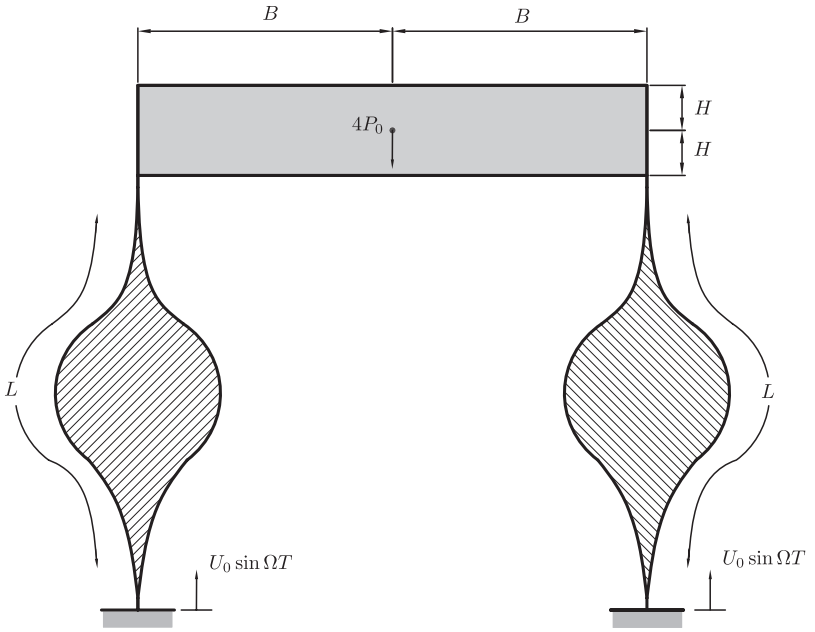

Fig. 9. Geometry of rigid bar with two-column isolators.

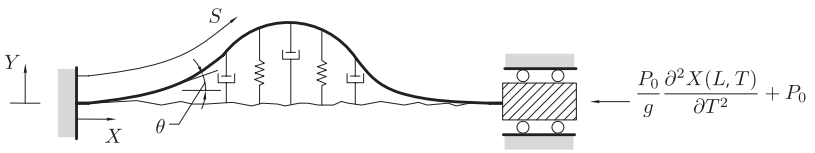

Fig. 10. Geometry of column drawn horizontally.

does not rotate during steady-state vibration. The isolators remain vertical, their ends move up and down, and the two columns in each isolator are mirror images of each other. The horizontal components of the distributed stiffness and damping forces of the filler on the columns are assumed to dominate, and the vertical components of the filler's forces are neglected in the analysis.

For each isolator, a single column will be analyzed, as depicted in Fig. 10 in a horizontal configuration with distributed springs and dashpots. The column is assumed to be unstrained when the rotation angle $\theta = \theta_0(S)$ is given by

$$\theta_0(S) = d_0 \sin \frac{2\pi S}{L}. \tag{22}$$

The corresponding deflection $Y_0(S)$ is approximately equal to the first buckling mode of a fixed–fixed column with amplitude $d_0 L/\pi$. The distributed stiffness is assumed to be linear in the additional deflection $Y - Y_0$ and to be inversely proportional to Y_0, so that the filler is stiffer where it is thinner. The distributed damping is assumed to be proportional to the transverse velocity $\partial Y/\partial T$ and to Y_0, so that the damping is greater where the filler is thicker. External damping is neglected in this case.

The governing equations for the column are

$$\frac{\partial X}{\partial S} = \cos\theta, \quad \frac{\partial Y}{\partial S} = \sin\theta, \quad \frac{\partial \theta}{\partial S} = \frac{M}{EI_c} + \frac{d\theta_0}{dS}, \quad \frac{\partial M}{\partial S} = Q\cos\theta - P\sin\theta,$$
$$\frac{\partial P}{\partial S} = -\mu\frac{\partial^2 X}{\partial T^2}, \quad \frac{\partial Q}{\partial S} = -\mu\frac{\partial^2 Y}{\partial T^2} - 2C_f Y_0 \frac{\partial Y}{\partial T} - \frac{2K_f}{Y_0}(Y - Y_0), \quad \frac{dY_0}{dS} = \sin\theta_0, \tag{23}$$

where K_f and C_f are constant stiffness and damping coefficients. The time-dependent variables are written in a form similar to Eq. (2), and the nondimensionalized quantities in Eq. (20) are used, without the subscript j, along with

$$y_0 = \frac{Y_0}{L}, \quad k_f = \frac{2K_f L^3}{\mathrm{EI}_c}, \quad c_f = \frac{2C_f L^3}{\sqrt{\mu \mathrm{EI}_c}}. \tag{24}$$

The transmissibility in this case is defined by

$$TR = \frac{1}{U_0}\sqrt{\{\mathrm{Re}\,[X_d(L)]\}^2 + \{\mathrm{Im}\,[X_d(L)]\}^2}. \tag{25}$$

5. Results for two-column isolators

The parameters in Eq. (21) are used again, except that $c = 1$ is replaced by $c_f = 1$, and other values for p_0 will be considered in the final figure. In the computer programs, the denominator y_0 in the stiffness force is replaced by $y_0 + 10^{-7}$ to avoid possible numerical problems near the column ends where $y_0 = 0$. The numerical procedure is similar to that for the symmetric case of the single-column isolators, with the addition in the equilibrium analysis of the condition $y_0(0) = 0$, a differential equation involving $q_e(s)$, and variation of $q_e(0)$ as well as $m_e(0)$.

Initial amplitudes d_0 of θ_0 are chosen as 0.01, 0.05, and 0.10, which, respectively, correspond to maximum (central) values 0.00318, 0.0159, and 0.0318 of the pre-bent deflection y_0. In equilibrium, the maximum value of y_e depends on p_0, k_f, and d_0. For example, if $p_0 = 40$, $k_f = 0.1$, and $d_0 = 0.1$, then $y_e(0.5) = 0.28$ [14].

The effect of the filler stiffness on TR is illustrated in Fig. 11, where $d_0 = 0.05$. As k_f increases from 0.1 to 1.0 and 10.0, the first peak moves from $\omega = 0.898$ to 1.612 and 15.82, and the second peak occurs at $\omega = 44.83$, 45.77, and 84.59, respectively. In Fig. 11, the largest range of applied frequency for which TR is small occurs for the lowest value of filler stiffness considered.

Fig. 12 depicts the influence of the size of the initial curvature of the columns on TR. In this case, $k_f = 0.1$. The first peak for $d_0 = 0.01$, 0.05, and 0.10, respectively, occurs at $\omega = 2.287$, 0.898, and 0.922. The transmissibility is usually lowest for the middle case $d_0 = 0.05$ in the range $1 < \omega < 45$.

For the single-column isolators, the weight of the bar was assumed to be high enough to buckle the columns. The two-column isolators, however, are pre-bent, and small supported weights also can be considered. In Fig. 13, values $p_0 = 10$, 20, and 30 are considered in addition to $p_0 = 40$. Here $k_f = 0.1$ and $d_0 = 0.1$. The value of ω at the first peak of TR increases as p_0 decreases; for $p_0 = 40$, 30, 20, and 10, respectively, it is at $\omega = 0.922$, 2.259, 6.488, and 13.34. The second peak for $p_0 = 40$, 30, and 20, respectively, occurs at $\omega = 44.60$, 49.17, and 53.67, but the case $p_0 = 10$ does not have a noticeable peak in that region. On the right side of Fig. 13, the peaks for these

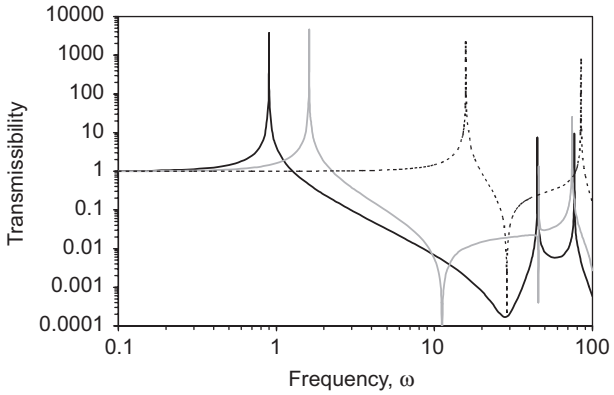

Fig. 11. Transmissibility curves for asymmetric bar with $d_0 = 0.05$, $0.1 < \omega < 100$: dark solid curve, $k_f = 0.1$; light solid curve, $k_f = 1.0$; and dotted curve, $k_f = 10.0$.

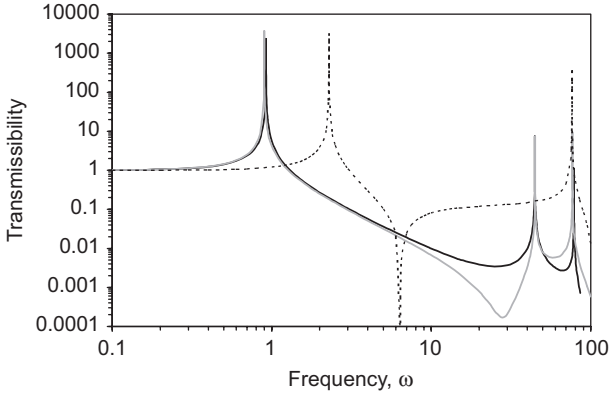

Fig. 12. Transmissibility curves for asymmetric bar with $k_f = 0.1$, $0.1 < \omega < 100$: dark solid curve, $d_0 = 0.1$; light solid curve, $d_0 = 0.05$; and dotted curve, $d_0 = 0.01$.

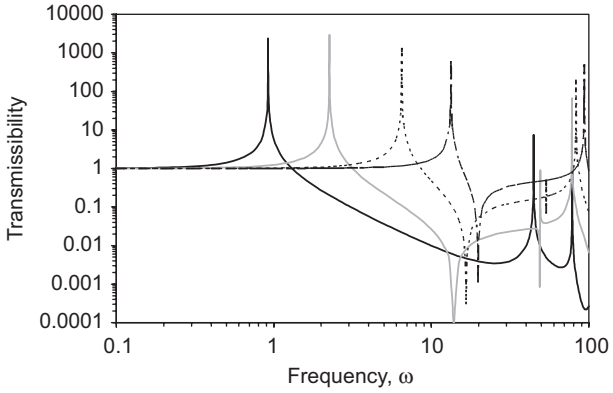

Fig. 13. Transmissibility curves for asymmetric bar with $k_f = 0.1$, $d_0 = 0.1$, $0.1 < \omega < 100$: dark solid curve, $p_0 = 40$; light solid curve, $p_0 = 30$; dotted curve, $p_0 = 20$; and dash-dot curve, $p_0 = 10$.

decreasing values of p_0 are at $\omega = 78.53$, 78.12, 82.98, and 93.45, respectively. The lowest transmissibility in the frequency range $1 < \omega < 100$ in Fig. 13 usually occurs for $p_0 = 40$.

6. Concluding remarks

The effectiveness of an isolator for a given system typically depends on the excitation. Simple-harmonic, vertical base motion was assumed, and a horizontal bar was supported at its ends by buckled columns or pairs of pre-bent columns bonded together. The bar was constrained against horizontal motion, so its coordinates were the vertical motion of the center of mass and rotational motion about the center of mass. Each column was modeled as an inextensible elastica, and a shooting method was applied to obtain numerical solutions. The transmissibility for the vertical deflection of the center of mass was plotted as a function of the excitation frequency. Since the columns were treated as continuous structural components, the transmissibility has an infinite number of peaks, but only a certain low range of frequencies was considered.

The range of frequencies for which the transmissibility is low (e.g., less than 0.1) depends on the system parameters. For the single-column isolators, asymmetry introduces an additional transmissibility peak between the first and second peaks for the symmetric case. Since the symmetric case is idealistic, with imperfections occurring in practice, the results for asymmetric cases should be more meaningful, and these cases have a reduced range of frequencies for which the transmissibility is low.

The two-column, pre-bent isolators can be used for loads below the buckling load, but are usually less effective for such cases if the excitation frequency is relatively low. If the curvature of the columns is decreased,

or if the stiffness of the filler is increased, the range of frequencies for effective isolation tends to move to higher frequencies.

Part 2 of this investigation presents an analysis of a square, rigid plate with pairs of pre-bent columns supporting each corner of the plate [15].

Acknowledgments

This research was supported by the US National Science Foundation under Grant no. CMS-0301084. The authors are grateful to the reviewers for their helpful comments.

References

[1] J. Winterflood, T. Barber, D.G. Blair, Using Euler buckling springs for vibration isolation, *Classical and Quantum Gravity* 19 (2002) 1639–1645.

[2] J. Winterflood, D.G. Blair, B. Slagmolen, High performance vibration isolation using springs in Euler column buckling mode, *Physics Letters A* 300 (2002) 122–130.

[3] J. Winterflood, T.A. Barber, D.G. Blair, Mathematical analysis of an Euler spring vibration isolator, *Physics Letters A* 300 (2002) 131–139.

[4] J.C. Dumas, K.T. Lee, J. Winterflood, L. Ju, D.G. Blair, J. Jacob, Testing of a multi-stage low-frequency isolator using Euler spring and self-damped pendulums, *Classical and Quantum Gravity* 21 (2004) S965–S971.

[5] E.J. Chin, K.T. Lee, J. Winterflood, L. Ju, D.G. Blair, Low frequency vertical geometric anti-spring vibration isolators, *Physics Letters A* 336 (2005) 97–105.

[6] L.N. Virgin, R.B. Davis, Vibration isolation using buckled struts, *Journal of Sound and Vibration* 260 (2003) 965–973.

[7] R.H. Plaut, L.A. Alloway, L.N. Virgin, Nonlinear oscillations of a buckled mechanism used as a vibration isolator, in: G. Rega, F. Vestroni (Eds.), *IUTAM Symposium on Chaotic Dynamics and Control of Systems and Processes in Mechanics*, Springer, Dordrecht, The Netherlands, 2005, pp. 241–250.

[8] R.H. Plaut, J.E. Sidbury, L.N. Virgin, Analysis of buckled and pre-bent fixed-end columns used as vibration isolators, *Journal of Sound and Vibration* 283 (2005) 1216–1228.

[9] P. Bonello, M.J. Brennan, S.J. Elliott, Vibration control using an adaptive tuned vibration absorber with a variable curvature stiffness element, *Smart Materials and Structures* 14 (2005) 1055–1065.

[10] J. Jiang, E.M. Mockensturm, A motion amplifier using an axially driven buckling beam: I. Design and experiments, *Nonlinear Dynamics* 43 (2006) 391–409.

[11] S. Wolfram, *The Mathematica Book*, Third ed, Cambridge University Press, Cambridge, UK, 1996.

[12] R.H. Plaut, R.P. Taylor, D.A. Dillard, Postbuckling and vibration of a flexible strip clamped at its ends to a hinged substrate, *International Journal of Solids and Structures* 41 (2003) 859–870.

[13] S.T. Santillan, L.N. Virgin, R.H. Plaut, Postbuckling and vibration of heavy beam on horizontal or inclined rigid foundation, *Journal of Applied Mechanics* 73 (2006) 664–671.

[14] H.M. Favor, Two-dimensional Analysis of Vibration Isolation of Rigid Bar Supported by Buckled or Pre-bent Struts, MS Thesis, Virginia Polytechnic Institute and State University, Blacksburg, VA, 2004 〈http://scholar.lib.vt.edu/theses/available/etd-12132004-205927〉.

[15] A.E. Jeffers, R.H. Plaut, L.N. Virgin, Vibration isolation using buckled or pre-bent columns, part 2: three-dimensional motions of horizontal rigid plate, *Journal of Sound and Vibration*, doi:10.1016/j.jsv.2007.09.039.